DOI: 10.1002/smll.200600211

Flowing Lattices of Bubbles as Tunable, Self-Assembled Diffraction Gratings

*Michinao Hashimoto, Brian Mayers, Piotr Garstecki, and George M. Whitesides**

***W**e demonstrate tunable, fluidic, two-dimensional diffraction gratings based on a microfluidic platform comprising a flow-focusing bubble generator and flowing, regular lattices of bubbles formed by dynamic self-assembly. The structure of these lattices can be tuned with switching times of less than ten seconds by changing the pressures and rates of flow applied to the device. These diffraction gratings exhibit high stability (over hours of operation if properly designed and operated). For our devices, we achieved tunable ranges in pitch from 12 to 51 μm, corresponding to first-order diffraction angles from 3.2° to 0.7° for light with a wavelength of 632 nm.*

Keywords:
- bubbles
- diffraction gratings
- flow focusing
- microfluidics
- self-assembly

1. Introduction

This paper demonstrates tunable and reconfigurable diffraction gratings composed of lattices of bubbles flowing in water containing a surfactant in microfluidic channels. Control over the size and volume fraction of the bubbles is demonstrated to control the structure of flowing, regular lattices of bubbles that form by self-assembly.[1] These flowing lattices can be well ordered and stable, and their geometries and lattice constants can be tuned in real time with switching times of less than ten seconds. Two types of microfluidic devices are demonstrated, which generate two-, and one-dimensional diffraction patterns, respectively. The diffraction patterns are stable for extended periods of time (seconds to hours), with a pitch tunable from 12 to 51 μm. Here, the pitch denotes the periodicity of the self-assembled structure, determined by the apparent diameter of each bubble in the microfluidic channel. The corresponding range of the angle of the first-order diffraction peak for perpendicularly incident light at $\lambda = 632$ nm is from 3.2° to 0.7°. Such tunable diffraction gratings can be used to 1) direct monochromatic light into a specified angle, and adjust this angle dynamically, 2) sweep the angles of the diffracted beams at specified angular velocity, and 3) split multimodal light into separate, monochromatic beams, and change the color of the light diffracted at a particular angle dynamically.

Optical components (diffraction gratings, lenses, and mirrors) are typically fabricated from rigid materials such as glass, quartz, rigid polymers, or metals. Specific applications, however, may require optics that can be modified structurally in real time, that is, "adaptive optics". There have been several demonstrations of deformable solid optical components for the modulation of light.[2–8] Fluid-based optical components represent a class of components that is intrinsically well suited for dynamic, reversible control over optical properties.[9–23] The adjustable parameters include both the geometry of the active components (e.g., the diameter of the core, in a liquid–liquid waveguide), and the property of the materials of which they are made (e.g., indices of refraction of liquid, as controlled by the concentration of salts dis-

[*] M. Hashimoto, Dr. B. Mayers, Prof. Dr. P. Garstecki, Prof. Dr. G. M. Whitesides
Department of Chemistry and Chemical Biology
Harvard University
12 Oxford St., Cambridge, MA (USA)
Fax: (+1) 617-495-9857
E-mail: gwhitesides@gmwgroup.harvard.edu
Prof. Dr. P. Garstecki
Institute of Physical Chemistry, Polish Academy of Sciences
Kasprzaka 44/52, 01-224 Warsaw (Poland)

Supporting information for this article is available on the WWW under http://www.small-journal.com or from the author.

NANO MICRO small

solved in them, or absorbance, as controlled by concentrations of dyes).

The use of immiscible fluids (emulsions, dispersions and foams) provides an additional route to periodic, self-assembled geometries. Microfluidic devices allow sensitive control over the process of formation of both gas–liquid[1,24] and liquid–liquid dispersions,[25–27] with the size of the discrete fluid elements and the volume fraction of the dispersed phase as easily tunable parameters. At high volume fractions of the bubbles or droplets in the continuous phase, these elements of fluid often self-assemble into highly regular, periodic patterns. Bragg and Nye originally described the assembly of millimeter-size, monodisperse bubbles into hexagonal patterns.[28] Gañán-Calvo and co-workers later reported the self-assembly of micrometer-sized bubbles into so-called "meso-crystals".[24,29] Recently, van der Net described detailed three-dimensional lattice structures of such meso-crystals composed of gas bubbles.[30] Lattices of bubbles in microfluidic platforms have two attractive features: 1) the lattices can be highly regular; 2) the lattice parameters can be tuned by appropriate changes in externally controlled pressure gradients. Diffraction from static lattices of droplets has already been demonstrated.[31] Here we explore the use of flowing lattices in microchannels as diffracting elements in situ, and demonstrate that the geometry of these lattices can be controlled in real time by changing the flow parameters of the liquid and vapor phases.

The use of a microfluidic, flow-focusing bubble generator to prepare a flowing, regular lattice of bubbles is described, as well as a description of the diffraction of visible light by these lattices. The dynamic response of the system, and of the corresponding diffraction patterns is discussed, along with changes in the rate of flow and pressure applied to the system. Concluding remarks pertaining to the potential applications of this system, and on its possible extensions, are then given.

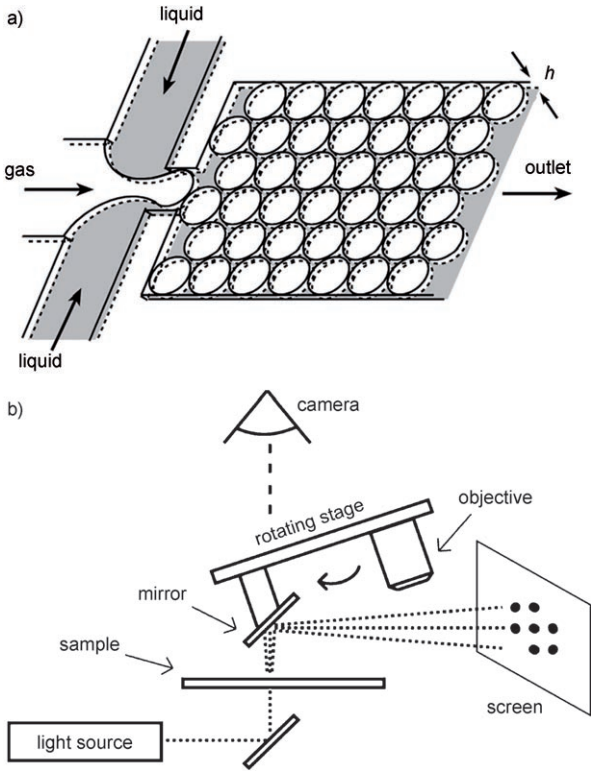

Figure 1. Schematic representations of the experimental setup. a) The flow-focusing bubble generator and self-assembled lattice of bubbles: A tank of nitrogen gas connects to the gas inlet, and digitally controlled syringes connect to the liquid inlets. The system generates monodisperse bubbles that pack into a quasi-two-dimensional sheet. Cylindrical bubbles at high volume fraction pack to form a hexagonal lattice in the outlet channel. The symbol *h* denotes the height of the outlet channel. b) Diffraction and display of incident laser beam: Diffracted laser light orthogonal to the plane of the bubble lattice is displayed on a white screen. "Sample" denotes the self-assembled flowing lattice of bubbles. The objectives are switched to observe the sample and to display the corresponding diffraction pattern.

2. Results and Discussion

Our group along with the groups of Stone, Anna, Gañán-Calvo, and others have previously described the formation of bubbles in a microfluidic flow-focusing (FF) geometry (Figure 1a).[1,24,26,32–35] Briefly, the FF region comprises two inlet channels for the liquid phase and a single inlet channel for the gaseous phase. The gas and liquid phases meet at a junction upstream of a narrow orifice. The gaseous thread periodically enters the orifice, breaks, and releases a bubble into the outlet channel. The volume of the bubble and the volume fraction of the dispersed phase can be independently controlled by adjusting the pressure p applied to the gas stream, and the rate of flow Q of the liquid.[1] Such control is used to prepare dispersions of bubbles of various sizes and volume fractions. The outlet channel – in which the flowing diffraction gratings are formed – is typically much wider (width $w \approx 1$ mm) than tall (height $h \approx 10$–20 μm). In this geometry, the bubbles are squeezed between the top and bottom walls of the channel and adopt flattened, disklike shapes (Figure 1a). In order to minimize their interfacial area, these flattened bubbles preserve circular cross sections in the plane of the channel. At high volume fractions,[36] bubbles contact each other and interact by shape-restoring elastic forces. These interactions lead to the self-assembly of bubbles into ordered two-dimensional lattices.[27]

For a fixed rate of flow of the continuous phase (the aqueous solution of surfactant), as the pressure applied to the stream of gas is increased, two simultaneous processes are observed: 1) The size of the bubbles increases (the volume of an individual bubble (V_b) is proportional to the ratio of the applied pressure and the rate of flow of continuous phase, $V_b \propto p/Q$),[1] and 2) the volume fraction of the bubbles in the outlet channel (ϕ_{vol}; $0 < \phi_{vol} < 1$) increases. The flow-focusing bubble generator allows the volume fraction of bubbles in the continuous liquid to be controlled continuously over a broad range. A change in the rate of flow of the continuous fluid, and in the pressure applied to the stream of gas, immediately affects the process of the formation of bubbles. The time needed to introduce and stabi-

lize a new lattice structure in the channel depends on the magnitude of change in the flow parameters (larger changes require longer time to restore stable operation), and range from milliseconds to seconds.

At low volume fractions the bubbles flowed in disordered packs (Figure 2a). As ϕ_{vol} increased, the packs organized into hexagonal packed domains. These domains continuously reorganized – interchanging bubbles between each other, changing their size, and rotating – as they flowed downstream. At volume fractions that approached the limit of the packing of disks on the plane (0.91), the domains fused into a single lattice extending throughout the outlet channel (Figure 2b–d). For ϕ_{vol} between $\approx$0.80 and $\approx$0.90, dislocation lines were observed that moved as the lattices flowed downstream (Figure 2b). A further increase in the applied pressure of the gas ($\phi_{vol} \approx 0.91$) caused the bubbles to fill the entire plane of the channel (with the liquid confined to the curved spaces between bubbles; similar to the Plateau borders)[37] and the defects in the lattices were minimized (Figure 2c and d). At a maximum volume fraction of gas, however, the system still never displayed perfect hexagonal packing. Regions of incomplete packing of bubbles remained, and the structure of the lattice was unstable around such defects (Figure 2e). The packing of bubbles underwent constant reorganization as the bubbles flowed downstream. Since the system flowed continuously, defects continuously entered and exited the observation zone.

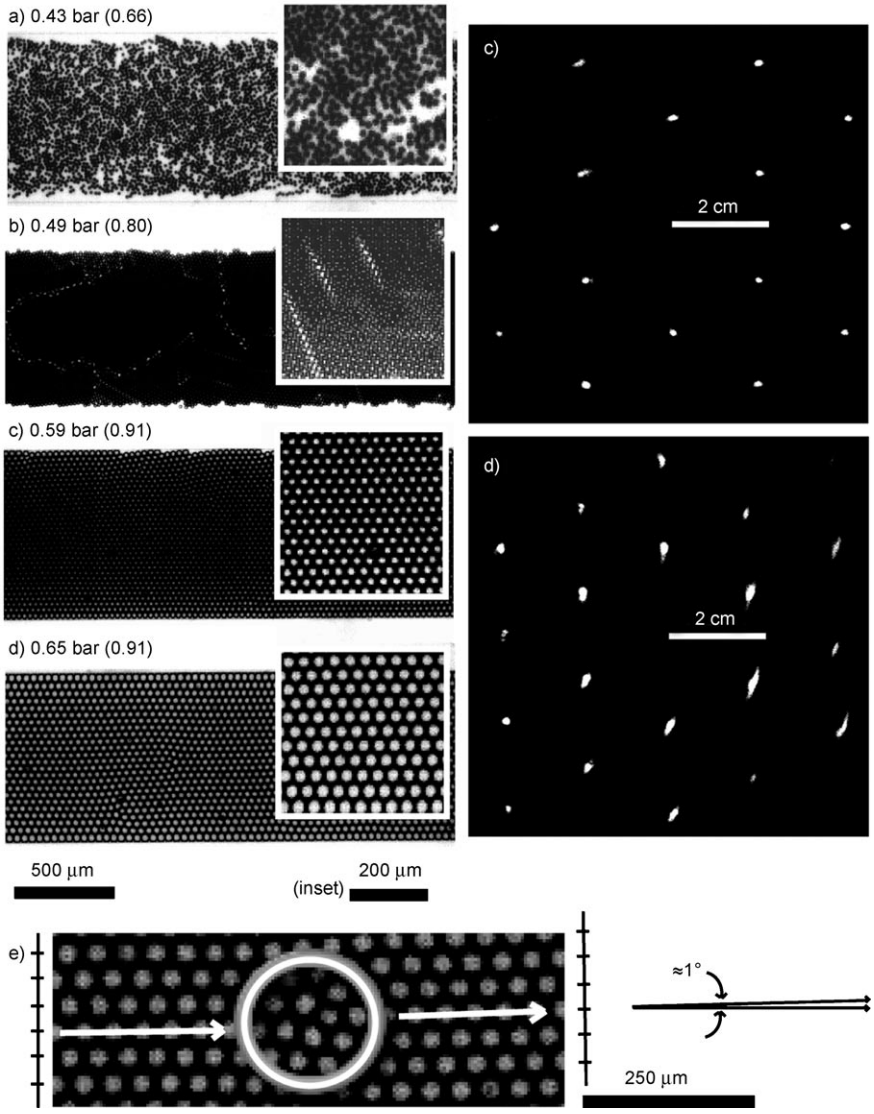

Figure 2. Packing of bubbles in a straight outlet channel that was 1-mm wide and 16-µm high. The rate of flow of the continuous phase was 0.028 µL s^{-1}. The numbers in parentheses denote the volume fraction of bubbles (ϕ_{vol}). a) 0.43 bar, $\phi_{vol} = 0.66$; the volume fraction of the bubbles was not sufficiently high to pack the outlet channel. b) 0.49 bar, $\phi_{vol} = 0.80$; bubbles packed as a loose lattice with linear defects and constantly reorganized the domain of packing as they flowed downstream. c) 0.59 bar, $\phi_{vol} = 0.91$, and d) 0.65 bar, $\phi_{vol} = 0.91$; stable packed lattices of bubbles with lattice constants of c) 34 µm and d) 51 µm (left), and their corresponding diffraction patterns (right). e) A defect in a 'stable' lattice. Even under the optimal conditions, these lattices contained occasional defects that slightly change the orientation of the lattice. The structure in the frame corresponding to 0.65 bar shows a defect (a hole) that changes the orientation of the packing. The lattice spacing remained the same, but the lattice shifted by approximately one half of the unit cell and reoriented locally. The two white arrows show the orientation of the alignment of bubbles upstream and downstream of the hole. The orientations are off by $\approx 1^\circ$ in this example.

The self-assembled, tunable, lattices were used as diffraction gratings. These gratings can be modeled as both amplitude gratings and phase gratings. The menisci of the bubbles refract the incident light radially, similar to diffraction from periodic arrays of dots or holes (amplitude gratings). The bubbles and the continuous medium also represent periodic arrays of alternating refractive indices (phase gratings). In a phase grating, the intensity of light at each diffraction spot is modulated by changing the phase difference of rays of interfering light that passes through the grating. In these experiments, the height of the channel (10–20 µm) and the refractive index of our continuous liquid phase (water, $n_D = 1.33$), and the wavelength of light (He/Ne laser, 632 nm) determine the phase shift of the diffracted light. These parameters can be adjusted with relative ease – for example, changing the refractive index of the continuous phase by adding salts or by changing its temperature – to optimize the efficiency of the grating at a particular wavelength. In this paper, the focus is on the ability to adjust the periodicity (d) of the grating and the resultant changes in the deflection of incident radiation.

NANO MICRO small

The stability of the resulting diffraction pattern depends on the volume fraction of the bubbles (ϕ_{vol}) in the outlet channel. A low volume fraction results in incomplete packing of lattices that creates multiple domains of two-dimensional hexagonal lattices. These domains were oriented in different directions, and the orientations of the resulting diffraction patterns differ accordingly. In these experiments, the incident laser beam was directed through a fixed location of the microfluidic channel at which the lattice of bubbles was constantly flowing. As the border of a domain passed through this location, the diffraction pattern would appear to rotate, or radially fluctuate over time.

Figure 3 shows the influence of the volume fraction of bubbles on the stability of the diffraction patterns. Figure 3a (i) is an example of the packing of the bubbles at an intermediate volume fraction ($0.80 < \phi_{vol} < 0.90$). At this range of volume fraction, the walls did not stabilize the packing of the lattice, and it was typical for a number of defects to persist in the lattice. At the maximum volume fraction ($\phi_{vol} \approx 0.91$, Figure 3a (ii)), it was possible to completely annihilate discrete borders of domains. This condition of maximum volume fraction maximized the stability of the diffraction pattern for this geometry of the channel. However, a small fraction ($\approx 0.1\,\%$) of misplaced bubbles were still observed to disturb the packing of the lattice.

The stability of the diffraction pattern was characterized using two parameters; the angle θ of orientation of the diffraction pattern, and the angle ϕ of the first-order diffraction (FOD) peak. Figure 3b and c shows θ and ϕ for 632-nm light over a period of 30 min with the system at steady state at two different pressures to show the effects of ϕ_{vol} on the stability of the diffraction pattern. At $\phi_{vol} \approx 0.91$, the standard deviation of the orientational angle (σ_θ) is 1.7° (2.8% of 60°, the degenerate angle of the hexagonal pattern). Fluctuations in the FOD angle at $\sigma_\phi = 0.02°$, equivalent to 2.1% of the mean FOD angle, were measured under optimized conditions. At $\phi_{vol} \approx 0.82$, σ_θ nearly doubles, as does σ_ϕ (Figure 3d). Diffraction efficiencies of 3% (measured as the ratio of the intensity of a single spot to the total intensity of the incident beam) have been observed. In comparison, commercial transmission gratings include those having efficiencies of 17% (GT-12 (Thorlab) with an FOD angle of 49.3°) and 67% (GT-03 (Thorlab) with an FOD angle of 10.9°) for 632 nm light.[38]

Thus far, the outlet channel of our systems was designed with $w = 1$ mm to allow straightforward positioning of the laser beam onto the lattice. With this wide channel, however, if the size of each bubble was small, the walls did not adequately constrain the packing of the bubbles over the span of the channel even though the

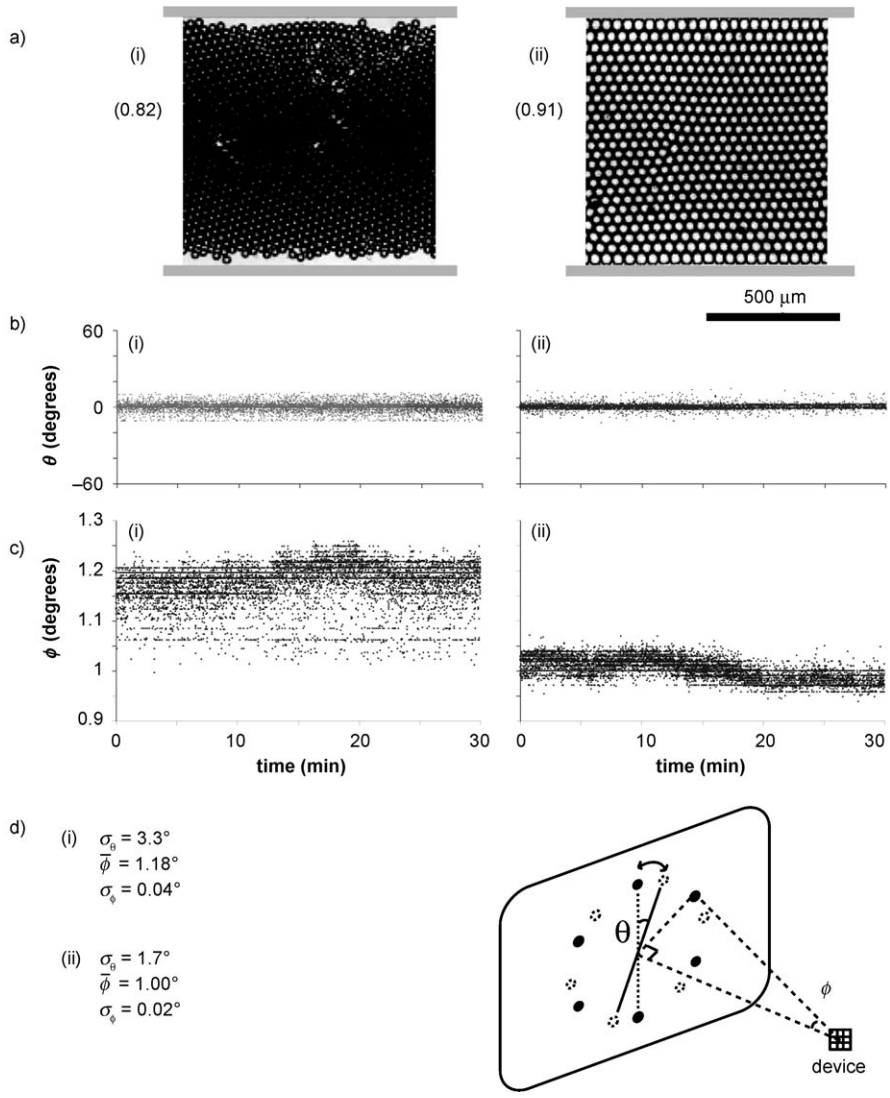

Figure 3. Stability of diffraction pattern from i) a loose lattice undergoing reorganization ($\phi_{vol} \approx 0.82$) and ii) a lattice of bubbles under optimal conditions ($\phi_{vol} \approx 0.91$). The pressure of nitrogen (p) and the rate of flow of water (Q), denoted by [Q(μL s^{-1}), p(bar)], were i) [0.056, 0.50] and ii) [0.056, 0.63]. a) Optical micrographs of the characteristic structures of bubbles for each set of parameters. b) Fluctuation of the orientation of the diffraction pattern (θ) over 30 min. The average orientational angle was set to be zero. c) Fluctuation of the first-order diffraction (FOD) angle (ϕ) over 30 min. d) Summary of averages and errors for θ and ϕ. The sketch shows schematic representations of θ and ϕ.

volume fraction of bubbles was near maximum. Bubbles near the center of the channel flowed faster than bubbles near the walls of the channel.

In order to pack bubbles with smaller diameters (12 μm) into an ordered structure across the width of a channel, a microfluidic device was constructed that was composed of an array of 16 parallel channels of smaller width (w = 200 μm), that is, five times smaller than the channels used in the work described so far. These channels were separated by 20-μm-wide walls (Figure 4a). The total width of this array is 3.5 mm. In these narrower channels, the bubbles with smaller diameters packed reliably into highly organized flowing lattices with a very low density of defects, and were stable over a wider range of flow conditions (values of p and Q). Figure 4b shows arrays of packed lattices of bubbles at high volume fraction ($\phi_{vol} \approx 0.91$ or greater). This architecture of the channel was able to support defect-free lattices with bubbles as small as 12 μm in diameter. The presence of the periodic wall, however, broke the hexagonal symmetry of the system.

The lattices were oriented with one of the base vectors of the hexagonal lattice pointing in the direction of the liquid flow, that is, parallel to the wall of the channels. In this direction, the periodicity of the lattice arises solely from the packing of the bubbles, so that the positions of the diffracted spots are the same as those for a 2D grating formed by

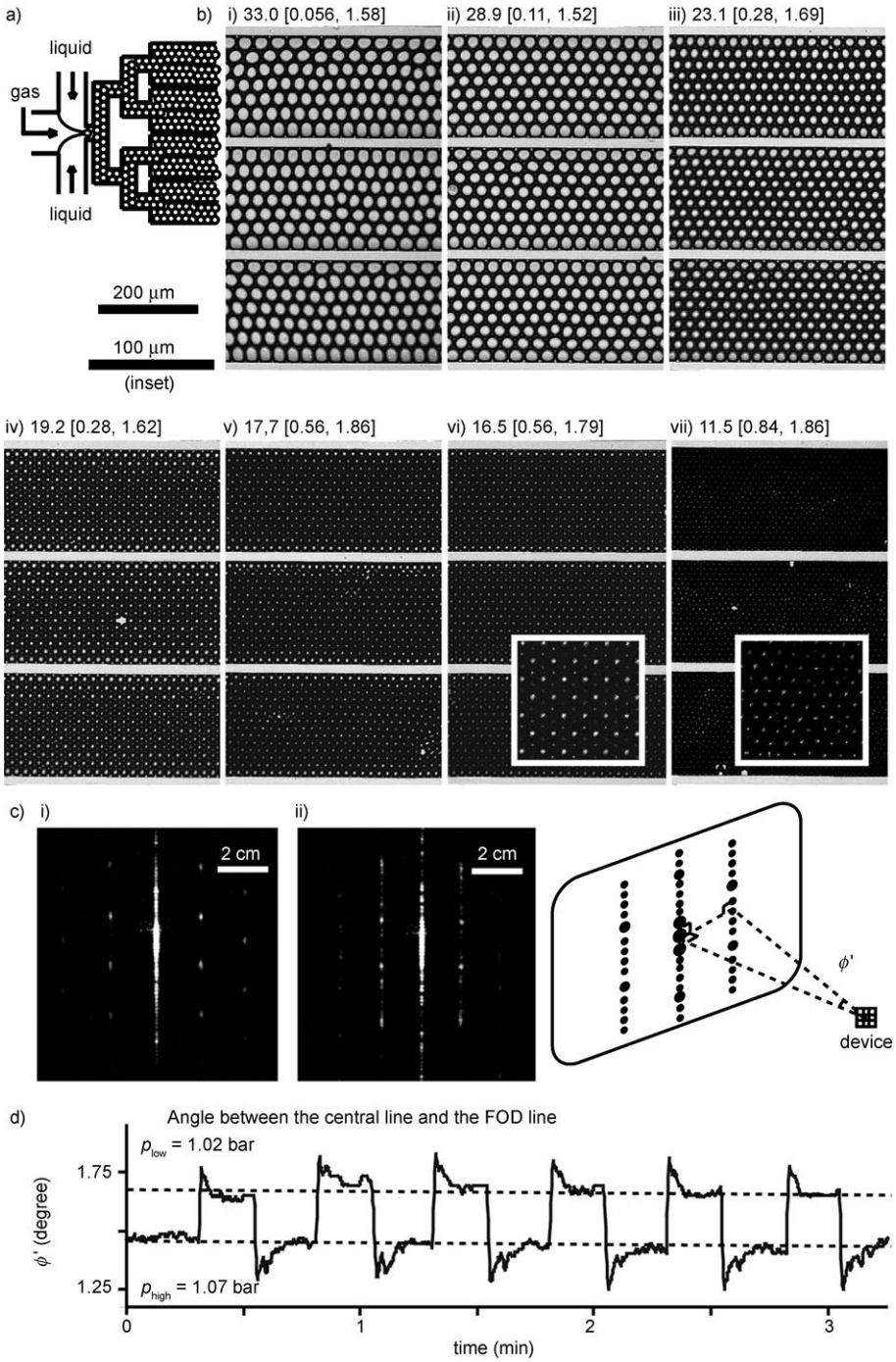

Figure 4. One-dimensional diffraction grating: a) A schematic representation of the outlet channel. Periodic poly(dimethylsiloxane) (PDMS) walls separated a wide outlet channel into multiple narrower outlet channels. The width of the spacers was on the same order as the diameter of the bubbles. b) Packing of the bubbles in the array of outlet channels. Each channel was 200-μm wide and 12-μm high; the spacer was 20-μm wide. The optical micrographs show three parallel channels. The insets show magnifications of a single-outlet channel. The figures above each micrograph indicate the diameter of bubbles (d), the rate of flow of water (Q), and the pressure of nitrogen (p), denoted as d (μm) [Q(μL s^{-1}), p(bar)]. c) Diffraction patterns from multiple parallel channels. Values of Q and p, denoted by [Q(μL s^{-1}), p(bar)], are i) [0.056, 1.29] and ii) [0.056, 1.17]. d) Real-time switching of applied pressure. The plot shows the distance between the central line and the FOD line. The applied pressure was manually alternated every 15 s between 1.07 bar and 1.02 bar, with the rate of water held constant at 0.42 μL s^{-1}, and the change in the diffraction pattern was recorded.

NANO MICRO small

bubbles assembled in a wide channel. In the direction perpendicular to flow, there are two sources of periodicity: One is associated with the periodicity of the lattice of bubbles, while the other is associated with the periodic arrangement of the parallel channels. This mixed periodicity makes the diffraction pattern associated with this direction indistinct, and the vertical spots are narrowly spaced, forming an almost continuous line (for example, the periodicity of the wall of the channel, 220 μm, yields diffracted spots separated by 0.16°, corresponding to 0.2 cm in our experimental setting, where the distance from the sample to the screen is 80 cm). We treated the system as a 1D diffraction grating with a pitch determined by the lattice of bubbles, and characterized the resulting diffraction pattern with the angle formed by such pseudo-lines (ϕ'; Figure 4). Note that ϕ' is smaller by a factor of $\sin 60^\circ$ than ϕ, which was used to characterize the 2D diffraction pattern obtained in the wide channel.[39] Figure 4c shows two such diffraction patterns.

The stabilizing effect of the walls of the channels on the lattice of bubbles allowed the demonstration of real-time switching of the 1D diffraction grating (Figure 4d). In this experiment the pressure applied to the stream of gas was changed every 15 s and the change in the angle formed by the central line and the FOD line (ϕ') was monitored. The system can be rapidly switched between states characterized by higher and lower pressure, p_{high} and p_{low}, respectively. Times required for equilibration upon the change in the pressure were 8 s or lower. The average values of ϕ' after attaining the equilibrium were $1.44 \pm 0.03^\circ$ and $1.67 \pm 0.03^\circ$ for the p_{high} state and the p_{low} state, respectively. This demonstrated that the use of narrower channels allowed bubbles of smaller diameter (<30 μm) to self-assemble reproducibly into ordered structures.

For all the devices that were prepared, the functional range of bubble sizes that could be generated, and that self-assembled into regular lattices, ranged from 12 to 51 μm. This range of sizes was determined by the width of the flow-focusing orifice (10 μm), the pressure of the applied gas, and the rate of flow of the liquid phase. This range in pitch translates to FOD angles for 632-nm light from 3.2° to 0.7°. We have demonstrated that such diffraction gratings, under optimized conditions, exhibit dynamic, reversible tunability with the change in the flow parameters, and high stability over an extended period of operation.

3. Conclusions

This paper describes the self-assembly of flowing streams of bubbles into functional, crystalline lattice structures, and the use of these lattices as tunable diffraction gratings. Previous work has demonstrated the tunability of diffraction gratings using elastomers,[2,5] liquid crystals,[31,40] photochemistry,[41] and electrochemistry.[42,43] We believe that these results provide the first example of a dynamic fluid–gas diffraction grating. This liquid–gas grating provides several characteristics that differ from familiar solid–liquid or solid–gas gratings: 1) reversible tunability in the periodicity of the grating; 2) reversible and dynamic control over the host liquid (both flow rate and composition) in real time; 3) generation and tunablility of a two-dimensional, isotropic diffraction pattern; 4) constant replacement of photobleached components.

There are two main disadvantages of the system. 1) the system requires handling liquids and compressed gases in addition to standard solid optical components. It is therefore less convenient to use than solid-state gratings; 2) the time required to switch the system from one structure to another is on the order of seconds; this value is much slower than that achieved by mechanical or electrical control of solid diffraction gratings. Nevertheless, the system should meet the demands for applications that do not require fast switching, such as optical sensing and bioassays.

Diffraction gratings are ubiquitous in optical and opto-analytical devices, such as lasers and spectrometers. We have previously described fluidic waveguides,[17] fluidic broadband light sources[18] and fluidic lasers.[22] The fluidic diffraction gratings described here will also contribute to the set of components available for use in fluidic optical systems, and for adaptive optical devices based on them.

4. Experimental Section

The channel system for the microfluidic devices were fabricated in a poly(dimethylsiloxane) (PDMS) slab using soft lithography,[44] and sealed this slab with a glass cover slide (Corning) by plasma oxidation to form the complete device.[45] It was ensured that the walls of the microchannels were hydrophilic by filling the channels with the aqueous solution of surfactant immediately after sealing.

An aqueous solution of Tween20 surfactant (2% w/w) was the liquid (continuous) phase, and nitrogen was the gas (dispersed) phase. A digitally controlled syringe pump (Harvard Apparatus, PhD2000 series) delivered the liquid to the device at a specified rate of flow. A pressurized tank provided the microfluidic device with gas at constant pressure via a needle valve and a digital manometer (Omega). A He/Ne laser ($\lambda = 632.8$ nm, $P =$ 3 mW) illuminated the center of the bubble lattice, with the direction of the beam perpendicular to the plane of the device 1 cm downstream from the flow-focusing bubble generator. The diameter of the beam was ≈ 1 mm. Diffraction patterns were projected onto a white screen located ≈ 80 cm from the plane of the microchannel. A Phantom V7 fast camera and a Nikon objective recorded still images and videos of the diffraction patterns. A Leica microscope and the same camera acquired images of the flowing lattices of bubbles.

In order to obtain sufficiently 'wide' lattices of bubbles to accommodate the width of the beam of the laser light, outlet channels were used that were up to $w \approx 1$ mm wide and $h \approx 10$ μm high. At such a low aspect ratio (h/w) the roof of the elastomeric microchannel is susceptible to collapse or deflection from internal pressure.[46] In order to avoid nonuniformities of the height of the channel resulting from this kind of deformation, one of the following two techniques was used: 1) Embedding a glass plate parallel to the roof of the channel in the PDMS slab to en-

hance the rigidity of the channel, and 2) redesigning the outlet channel with linear supports parallel to the direction of flow. (see the Supporting Information for details concerning the fabrication). With these approaches, defects were minimized in the structures of the lattices and thus functional, stable diffraction gratings were obtained over a wide range of flow parameters. Both techniques were successful; the first approach required extra steps in the fabrication, but allowed for the fabrication of a nondeformable channel with a low aspect ratio ($h/w \approx 100$). The second approach is simpler – it only required standard techniques for the preparation of microfluidic devices.[45] The channels prepared by the second approach were then used as one-dimensional diffraction gratings.

Acknowledgements

This work was supported by DOE award DE-FG02-OOER45852. Partial salary support for some of the work was provided by a DARPA subaward from the California Institute of Technology. P.G. thanks the Foundation for Polish Science for financial support.

[1] P. Garstecki, I. Gitlin, W. DiLuzio, G. M. Whitesides, E. Kumacheva, H. A. Stone, *Appl. Phys. Lett.* **2004**, *85*, 2649.
[2] J. L. Wilbur, R. J. Jackman, G. M. Whitesides, E. L. Cheung, L. K. Lee, M. G. Prentiss, *Chem. Mater.* **1996**, *8*, 1380.
[3] H. Kuck, W. Doleschal, A. Gehner, W. Grundke, R. Melcher, J. Paufler, R. Seltmann, G. Zimmer, *Sens. Actuators A* **1996**, *54*, 536.
[4] O. J. A. Schueller, D. C. Duffy, J. A. Rogers, S. T. Brittain, G. M. Whitesides, *Sens. Actuators A* **1999**, *78*, 149.
[5] B. A. Grzybowski, D. Qin, G. M. Whitesides, *Appl. Opt.* **1999**, *38*, 2997.
[6] S. Sakarya, G. Vdovin, P. M. Sarro, *Sens. Actuators A* **2002**, *97–98*, 468.
[7] J. S. Wang, I. W. Jung, O. Solgaard, *Sens. Actuators A* **2004**, *114*, 528.
[8] S. Uma, R. Matusiak, D. L. Hecht, E. J. Shrader, *IEEE J. Sel. Top. Quantum Electron.* **2004**, *10*, 435.
[9] P. Dress, H. Franke, *Appl. Phys. B* **1996**, *63*, 12.
[10] A. Hanning, J. Westberg, J. Roeraade, *Electrophoresis* **2000**, *21*, 3290.
[11] P. Mach, M. Dolinski, K. W. Baldwin, J. A. Rogers, C. Kerbage, R. S. Windeler, B. J. Eggleton, *Appl. Phys. Lett.* **2002**, *80*, 4294.
[12] A. Datta, I. Y. Eom, A. Dhar, P. Kuban, R. Manor, I. Ahmad, S. Gangopadhyay, T. Dallas, M. Holtz, F. Temkin, P. K. Dasgupta, *IEEE Sens. J.* **2003**, *3*, 788.
[13] C. Kerbage, B. J. Eggleton, *Appl. Phys. Lett.* **2003**, *82*, 1338.
[14] F. Cattaneo, P. Mach, J. Hsieh, T. Krupenkin, S. Yang, J. A. Rogers, *Mater. Res. Soc. Symp. Proc.* **2003**, *741*, *9*.
[15] Y. Cheng, K. Sugioka, K. Midorikawa, *Opt. Lett.* **2004**, *29*, 2007.
[16] S. Kuiper, B. H. W. Hendriks, *Appl. Phys. Lett.* **2004**, *85*, 1128.
[17] D. B. Wolfe, R. S. Conroy, P. Garstecki, B. T. Mayers, M. A. Fischbach, K. E. Paul, M. Prentiss, G. M. Whitesides, *Proc. Natl. Acad. Sci. USA* **2004**, *101*, 12434.
[18] B. T. Mayers, D. V. Vezenov, V. I. Vullev, G. M. Whitesides, *Anal. Chem.* **2005**, *77*, 1310.
[19] D. V. Vezenov, B. T. Mayers, D. B. Wolfe, G. M. Whitesides, *Appl. Phys. Lett.* **2005**, *86*, 041104.
[20] R. S. Conroy, B. T. Mayers, D. V. Vezenov, D. B. Wolfe, M. G. Prentiss, G. M. Whitesides, *Appl. Opt.* **2005**, *44*, 7853.
[21] D. B. Wolfe, D. V. Vezenov, B. T. Mayers, G. M. Whitesides, R. S. Conroy, M. G. Prentiss, *Appl. Phys. Lett.* **2005**, *87*, 181105.
[22] D. V. Vezenov, B. T. Mayers, R. S. Conroy, G. M. Whitesides, P. T. Snee, Y. Chan, D. G. Nocera, M. G. Bawendi, *J. Am. Chem. Soc.* **2005**, *127*, 8952.
[23] S. Balslev, A. Kristensen, *Opt. Express* **2005**, *13*, 344.
[24] A. M. Gañán-Calvo, J. M. Gordillo, *Phys. Rev. Lett.* **2001**, *87*, 274501.
[25] T. Thorsen, R. W. Roberts, F. H. Arnold, S. R. Quake, *Phys. Rev. Lett.* **2001**, *86*, 4163.
[26] S. L. Anna, N. Bontoux, H. A. Stone, *Appl. Phys. Lett.* **2003**, *82*, 364.
[27] P. Garstecki, M. J. Fuerstman, H. A. Stone, G. M. Whitesides, *Lab Chip* **2006**, *6*, 437.
[28] L. Bragg, J. F. Nye, *Proc. R. Soc. London A* **1947**, *190*, 474.
[29] A. M. Gañán-Calvo, J. M. Fernandez, A. M. Oliver, M. Marquez, *Appl. Phys. Lett.* **2004**, *84*, 4989.
[30] A. van der Net, W. Drenckhan, I. Weaire, S. Hutzler, *Soft Matter* **2006**, *2*, 129.
[31] D. Rudhardt, A. Fernandez-Nieves, D. R. Link, D. A. Weitz, *Appl. Phys. Lett.* **2003**, *82*, 2610.
[32] T. Cubaud, C. M. Ho, *Phys. Fluids* **2004**, *16*, 4575.
[33] J. M. Gordillo, Z. D. Cheng, A. M. Gañán-Calvo, M. Marquez, D. A. Weitz, *Phys. Fluids* **2004**, *16*, 2828.
[34] Q. Y. Xu, M. Nakajima, *Appl. Phys. Lett.* **2004**, *85*, 3726.
[35] P. Garstecki, H. A. Stone, G. M. Whitesides, *Phys. Rev. Lett.* **2005**, *94*.
[36] Surface Coverage: The volume fraction of the bubbles in the outlet channel can be approximated by the fraction of the area of the floor of the channel occupied by the bubbles. The maximum packing fraction of disks on an unbounded plane is $\phi_{MAX} = \pi/(2\sqrt{3}) = 0.91$; in the presence of the walls, ϕ_{MAX} is smaller and the 'circular' bubbles self-organize into ordered lattices at values of ϕ that are slightly smaller than 0.91, with the exact value depending on the ratio of the diameter of the circular cross section of the bubble to the width of the channel.
[37] D. Weaire, S. Hutzler, *The Physics of Foams*, Clarendon Press, Oxford, **1999**.
[38] Thorlabs Product Catalog, Vol. 18, p. 655.
[39] ϕ and ϕ' are related by $\tan(\phi') = \sin(60^\circ)\tan(\phi)$. By the small-angle approximation, namely $\tan(x) \approx x$ for $x \ll 1$, we have $\phi' = \sin(60^\circ)\phi$.
[40] V. K. Gupta, N. L. Abbott, *Science* **1997**, *276*, 1533.
[41] S. Y. Bai, Y. Zhao, *Macromolecules* **2002**, *35*, 9657.
[42] T. S. Bergstedt, B. T. Hauser, K. S. Schanze, *J. Am. Chem. Soc.* **1994**, *116*, 8380.
[43] S. J. Tian, N. R. Armstrong, W. Knoll, *Langmuir* **2005**, *21*, 4656.
[44] Y. N. Xia, G. M. Whitesides, *Annu. Rev. Mater. Sci.* **1998**, *28*, 153.
[45] D. C. Duffy, J. C. McDonald, O. J. A. Schueller, G. M. Whitesides, *Anal. Chem.* **1998**, *70*, 4974.
[46] E. Delamarche, H. Schmid, B. Michel, H. Biebuyck, *Adv. Mater.* **1997**, *9*, 741.

Received: April 28, 2006
Published online on September 14, 2006

